Prediction of a novel topological multidefect ground state

Sergey Prosandeev, S. Prokhorenko, Y. Nahas, and L. Bellaiche

Phys. Rev. B **100**, 140104 — Published 28 October 2019

DOI: 10.1103/PhysRevB.100.140104

Prediction of a novel topological multi-defect ground state

Sergey Prosandeev[1,2], S. Prokhorenko[1], Y. Nahas[1], and L. Bellaiche[1]

[1] *Physics Department and Institute for Nanoscience and Engineering, University of Arkansas, Fayetteville, Arkansas 72701, USA*

[2] *Institute of Physics and Physics Department of Southern Federal University, Rostov-na-Donu 344090, Russia.*

Abstract

Atomistic first-principles-based effective Hamiltonian simulations are conducted in some ferroelectric system to predict the existence of a novel topological state. Such state is coined here "topological eclecton" because it is made of a plethora of electrical topological defects, including (i) vortices and antivortices in different planes, (ii) hedgehogs and anti-hedgehogs, and (iii) a few skyrmions. Such state can be a ground state and readapt itself to form other striking topological states or phases when, e.g., heating the system or applying electric fields. In addition to its unique combined topological characteristics, it is also ferroelectric and chiral in nature.

Various topological defects have been discovered in the last decades in different materials, which led to a deepening of topology in condensed matter[1,2] and to the design of novel devices[3–6]. For instance, in *magnetic* systems, vortices[6], antivortices[7], bubbles[4], bobbers[8,9], merons and skyrmions[10], were observed and predicted. Similarly, *electrical* vortices[11,12], antivortices[13], bubbles[14,15], dipolar waves[16,17], merons[17] and skyrmions[18,19] have been ecently found in ferroelectrics. Striking phenomena can also result when *different* topological defects coexist within the same state or phase, as, e.g., evidenced by the Berezinskii-Kosterlitz-Thouless phase possessing both vortices and antivortices[20–27]. Such complex topological defects can be also created in, e.g., nanodimers made of two spheres[28]. Another example is the prediction of creating spontaneously optically active materials when both electrical vortices and antivortices form[29].

Based on such facts and the existence of, e.g., the Schlieren textures of nematic liquid crystals that contain different types of topological defects (such as boojums and disclinations[30,31]), one can wonder if presently unknown states or phases possessing a *variety* of topological defects await to be discovered in dipolar systems. The aim of this Letter is to reveal that it is the case. As a matter of fact, we discover (in some ferroelectric system) a novel state that we coin as "topological eclecton", because of the eclectic occurrence of different vortices and antivortices, hedgehogs and anti-hedgehogs, and a few skyrmions. Such "topological eclecton" is presently found to be a *ground state*, and can generate other multi-defect states and phases when under external knobs, such as temperature and fields. It also possesses a spontaneous electric polarization and is chiral, which further emphasize its potential.

We employ here the effective Hamiltonian that was applied to $Ba_xSr_{1-x}TiO_3$ solid solutions[32] and compositionally graded systems[33], as well as to $BaTiO_3/SrTiO_3$ superlattices[34,35] and nanocomposites[13,18,36–39]. It reproduces some experimental data, such as the critical transition temperatures in $Ba_{0.5}Sr_{0.5}TiO_3$ disordered alloys[32] and the phenomenon and even magnitude of the temperature-gradient-induced polarization in $Ba_{0.75}Sr_{0.25}O_3$[40]. Effective Hamiltonian techniques have played a major role in the field of electrical topological defects by predicting electrical vortices[11], bubbles[14], dipolar waves[16], skyrmions[18], that have then been experimentally confirmed[12,15,17,19].

Here, we select 24×24×12 supercells that are periodic along all Cartesian directions, and inside which two $BaTiO_3$ (BTO) conical nanostructures are embedded in a $SrTiO_3$

(STO) matrix (STO should in fact be considered to be $(Ba_{0.15}Sr_{0.85})O_3$ here since our effective Hamiltonian predicts a paraelectric-to-ferroelectric transition of about 100K in STO[32]). These two cones are inverted with respect to each other, are connected to each other by their tips, and each have a radius of 33 Å for their common (x, y) base and a height (along the z-axis) of 23 Å (the x-, y- and z-axes are along the pseudo-cubic [100], [010] and [001] directions). Such nanostructure is reminiscent of InAs pyramid-like structures occurring inside a GaAs matrix[41,42], and of chains made of semiconductor quantum dots[43–47].

Our effective Hamiltonian is used within Monte-Carlo (MC) simulations by cooling the system. 20,000 MC sweeps are employed to equilibrate the system at each temperature, and then another 20,000 sweeps are used to compute thermodynamical averages. A particular output of simulations consists of the patterns of local modes (that are proportional to local electric dipoles) at each 5-atom site i, to be denoted by $\mathbf{u}_i$, at each MC sweep. Another extracted quantity is the toroidal moment of the local modes[48]:

$$\mathbf{G} = \left\langle \frac{1}{2N} \sum_i \mathbf{r}_i \times (\mathbf{u}_i - < \mathbf{u} >) \right\rangle \tag{1}$$

where $< \mathbf{u} >$ is the supercell average over the local modes, $\mathbf{r}_i$ is the position vector locating the i-th site, and N is the number of sites.

We also obtain generalized quadrupole moments of the density matrix[49]:

$$Q_{\alpha\beta} = \left\langle \frac{1}{2N} \sum_i (3 r_{i\alpha} r_{i\beta} - r_i^2 \delta_{\alpha\beta}) \rho_{i\alpha\beta} \right\rangle \tag{2}$$

where $\delta_{\alpha\beta}$ is the Kronecker symbol while $\rho_{i\alpha\beta} = (u_{i\alpha} - < u_\alpha >)(u_{i\beta} - < u_\beta >)$.

An Edwards-Anderson-like parameter is also determined as[50]:

$$q_u = \frac{1}{N} \sum_i \sum_\alpha \langle (u_{i\alpha} - < u_\alpha >) \rangle^2 \tag{3}$$

Quantities of Eqs (1)-(3) will help in identifying different phases.

Figures 1 report these calculated quantities and the supercell average of the local modes (that is proportional to the electrical polarization), for the investigated system on cooling from 600K to 10K with a step of 10K. Figures 2 show the projection of the pattern of the local modes into specific planes, as averaged over the last 20,000 MC sweeps for some temperatures, T.

The system is paraelectric and paratoroidic for T above $\simeq$ 340K since $< \mathbf{u} >$ and $\mathbf{G}$ both vanish there, in addition to the $Q_{\alpha\beta}$'s and q_u annihilating too. Such region is denoted as

Phase I. Upon cooling, another phase, to be coined Phase II, appears and extends from $\simeq$ 340K to about 250K. Phase II is characterized by the z-component of the toroidal moment getting finite, along with the Q_{xy} element of the density matrix and q_u also now deviating from zero, with these quantities strengthening in magnitude when decreasing T within Phase II. Such non-zero quantities reflect the emergence of electric vortices in (x, y) planes, as evidenced in Fig. 2c for the basal plane (Z=1) of BTO cones, therefore making Phase II ferrotoroidic. We therefore predict a phase transformation from paratoroidic to ferrotoroidic at $\simeq$ 340K. There is also no evident dipolar ordering in the (x, z) and (y, z) planes in Phase II, as indicated by the small and disordered arrows in Figs. 2a and 2b.

Another transition occurs at about 250K from Phase II to a new phase that we denote as Phase III. This latter phase is associated with the x- and y-components of the toroidal moment and the Q_{xz} and Q_{yz} quadrupoles all becoming finite. Phase III ranges from 250K to $\simeq$ 120K. The emergence of such finite quantities point out that, in addition to a persistent electrical vortex in the (x, y) basal planes (see Fig. 2f), another dipolar ordering is emerging in other planes. This is demonstrated by Figs. 2d and 2e revealing the existence of vortices lying in some (x, z) and (y, z) planes and made by two half-vortices, each located within adjacent BTO cones that are connected by the same base (half-vortices have been reported in magnetic systems[51]). Furthermore, the fact that that other adjacent cones are connected by their tip in our supercell has another topological implication in both (x, z) and (y, z) planes: such successive cones experience an antivortex-type of configuration near such tip (see circles in Figs 2d and 2e). Phase III can therefore be described as made of interconnected chains of vortices and antivortices in the (x, z) and (y, z) planes passing through the tip, along with dipole vortices in the (x, y) basal planes. We are not aware about any previous determination of such phase.

Upon further cooling, the average local mode adopts a $z-$component that becomes finite below $\simeq$ 120K, along with $x-$ and $y-$ components getting also finite but smaller in magnitude and of opposite signs between each other (see Fig. 1a). This marks the emergence of a new Phase coined as Phase IV and that, unlike Phase III, possesses a spontaneous polarization – therefore making Phase IV ferrotoroidic *and* ferroelectric. The x-, y- and especially the z-axis adopt both a finite component of the toroidal moment and of the polarization, which make Phase IV chiral in nature[11,18,39,52,53] and further emphasizes its potential applications. The x- and y-components of the toroidal moment are nearly independent of the

temperature in Phase IV (see Fig. 1b). The corresponding dipolar patterns of Phase IV are shown in Figs. 2(g), (h) and (i). The electric vortex in the (x, y) basal plane shown in Fig. 2(i) can now be considered to be made of four 90^0 domains rather than being circular as in Phases II and III, with the vortex core having slightly shifted with respect to the center of the base (because of the small in-plane electrical polarization). Moreover, Figs. 2g and 2h indicate that the appearance of a spontaneous polarization along the z-axis has rendered the half-vortices being asymmetric with respect to the z-line passing through the tips of the cone and also being less circular in shape (the z-component of the dipoles suddenly change of sign along the x or y-axis within the cones in Figs 2g and 2h, while the evolution of this component was more gradual in Figs 2d and 2e). The STO matrix has become polarized along the z-axis in Phase IV with up and down domains alternating along the y-axis in the (y, z) plane with the alternation taking place in the sites that are located half-ways (along the y-axis) between two successive rows of BTO cones – as evidenced by periodically repeating the pattern of Fig. 2h along the y-axis. Similar symmetrical features occur in the STO matrix in the (x, z) plane and along the x-axis (see Fig. 2g).

To further describe Phase IV at low temperature, we carried out topological characterization of its dipolar patterns at 10K. We computed several types of topological charges: (i) $S_1 \rightarrow S_1$ (circle to circle) winding number used to identify vortex- and anti-vortex-type point defects[2]; (ii) $S_2 -> S_2$ (sphere to sphere) winding number enabling the mapping of 3D point defects such as hedgehogs and anti-hedgehogs[2]; and finally (iii) $D_1 \rightarrow S_2$ (disk to sphere) Pontryagin's or skyrmion charge[54].

Results are displayed in Figs. 3(a)-(e), via schematization. Figure 3(c) confirms the presence of antivortices with their core being located at the meeting points of the cone tips in the (x,z) and (y,z) planes and of vortices with their core occurring inside the BTO cones at the meeting plane of the bases of such cones. The left side of the two snapshots of Fig. 3(c) also indicates other vortices and antivortices inside the STO matrix within (y,z) and (x,z) planes. Furthermore, Phase IV at low temperature possesses hedgehog-antihedgehog pairs (see Fig.3(d)). Interestingly, the hedgehog lies in close vicinity of the cones' tips: the center of the hedgehog is located at (12.5,10.5,5.5) in our (x,y,z) basis while the tip of the cone sits at (12.5,12.5,6.5). This hedgehog is somehow reminiscent of the Bloch point reported in magnetic bobber[9] since both the hedgehog and the Bloch point carry a +1 point topological charge in three-dimensions[55]. However and unlike the magnetic bobber, Phase

IV at low temperature only possesses skyrmions in some of its (x,y) planes, that are, in fact, located between the two (x,y) planes hosting the hedgehog and anti-hedgehog topological defects (the center of the anti-hedgehog is located at (8.5,14.5,9.5) in our (x,y,z) basis). Figures 3(e1) and 3(e2) show the distribution of the Pontryagin charge density within the (x,y)-planes in the full supercell and in those middle (x,y)-planes (defined by z=7, 8 and 9) hosting skyrmions, respectively. In these middle planes, the +1 skyrmionic charge is almost completely localized (see Fig. 3(e2)) at the junction of domain walls reversing the sign of x and y polarization components that yields the "central" vortex in the (x,y) planes, inside the BTO cone (see Fig. 2(i)). The remainder of the skyrmionic charge in (x,y) planes is located at the supercell boundaries inside of the STO matrix (see Fig. 2(i) and Fig. 3(e2)).

Phase IV thus harbors at low temperature a state that is endowed with a novel and exotic topological structure. We name it "topological electon" as regards to its "eclectic" topological nature made of vortices, antivortices, hedgehog, antihedgehog and few skyrmions. Such new and *ground* state may be of importance to design new type of non-volatile memory devices. Interestingly, phases possessing different topological defects are already known in several types of materials, but they are usually made of "only" two opposite of such defects, such as (i) vortices and antivortices making the so-called phase-locked state[13,56], or creating a gyrotropic state in some materials[29], or even being ingredients of the Berezinskii-Kosterlitz-Thouless phase[20–27]; and (ii) hedgehog and antihedgehog, extensively discussed in liquid crystals[57], cosmology[58], but also in ferroelectrics[59,60]. However, we are not aware that a topological state possessing so many different topological defects at the same time, as the "'topological electon" does, has ever been reported before. It will also be interesting in the future to reveal how these various topological defects interact with each other when under an *ac* probe, and likely yield unusual dynamical features[38,54,61].

Note also that Phase III can be considered to be a modification of the topological electon since we, e.g., numerically find that increasing the temperature disorganizes the structure, leading to a proliferation of hedgehogs and antihedgehogs, as well as small vortices and antivortices in (x,z) and (y,z) planes. Starting from this "topological electon" *and applying some external factors* can also result in other striking topological states and phases. For instance, yet another topologically non-trivial state, that is a "skyrmionic tube", can emerge from the topological electon upon application of an external electric field. This skyrmionic tube state is also composed of many topological defects and is topologically similar to that

of Ref.[18] (See Supplemental Material at[62]and References therein[18,39,52–54,63]).

In summary, we predict a novel topological state coined here "topological eclecton" and simultaneously possessing vortices, antivortices, hedgehogs, anti-hedgehogs and a few skyrmions. This "topological eclecton" is the ground state of the studied nanostructure[64], and is chiral in nature. It can also transform to other complex topological states and phases via the application of, e.g., temperature and fields. Note that we used here specific shapes (e.g., inverted cones) of a ferroelectric nanocomposite to make such state "easily" appearing, by creating a specific depolarizing electric field[11,14,18,37,39,65–69]. However, other types of ferroelectric nanostructures may also host the "topological eclecton", since we previously predicted an electric skyrmion in another nanocomposite[18] while it was then predicted in the simple $PbTiO_3$ material[70] and observed in ferroelectric superlattices[19]. We also hope that our study will encourage varying the shape of ferroelectric nanostructures to discover novel topological phases as well as will open a research field dedicated to studying interaction of various topological defects within the same phase. The "topological eclecton" may also exist in other types of materials (e.g., magnets, superfluids and superconductors) because of the existence of other interactions there that also favor the emergence of topological defects (such as Dzyaloshinskii-Moriya interactions[71] in magnets).

This work is supported by the DARPA Grant No. HR0011727183-D18AP00010 (TEE Program). L.B. thanks discussion with Prof. Blügel. S. P. appreciates support of RMES 3.1649.2017/4.6 and RFBR 18-52-00029_Bel_a.

[1] E. Bick and F. D. Steffen (Eds.), *Topology and geometry in physics*, Lect. Notes Phys. **659** (Springer, Berlin Heidelberg, 2005).

[2] N. D. Mermin, Mod. Phys. **51**, 591 (1979).

[3] J. Zhang, M. T. Albelda, Y. Liu, and J. W. Canary, Chirality **17**, 404 (2005).

[4] M. Prakash and N. Gershenfeld, Science **315**, 832 (2007).

[5] Y. Huang, W. Kang, X. Zhang, Y. Zhou, and W. Zhao, Nanotechnology **28**, 08LT02 (2017).

[6] S. D. Bader, Rev. Mod. Phys. **78**, 1 (2006).

[7] K. Shigeto, T. Okuno, K. Mibu, T. Shinjo, and T. Ono, Appl. Phys. Lett. **80**, 4190 (2002).

[8] F. Zheng, F. N. Rybakov, A. B. Borisov, D. Song, S. Wang, Z.-A. Li, H. Du, N. S. Kiselev, J. Caron, A. Kovács, M. Tian, Y. Zhang, S. Blgel and R. E. Dunin-Borkowski, Nature Nanotechnology **13**, 451 (2018).

[9] F. N. Rybakov, A. B. Borisov, S. Blügel, and N. S. Kiselev. Phys. Rev. Lett. **115**, 117201 (2015).

[10] X. Z. Yu, W. Koshibae, Y. Tokunaga, K. Shibata, Y. Taguchi, N. Nagaosa, and Y. Tokura, Nature **564**, 95 (2018).

[11] I. Naumov, L. Bellaiche, and H. Fu, Nature (London) **432**, 737 (2004).

[12] A. K. Yadav, C. T. Nelson, S. L. Hsu, Z. Hong, J. D. Clarkson, C. M. Schlep utz, A. R. Damodaran, P. Shafer, E. Arenholz, L. R. Dedon, D. Chen, A. Vishwanath, A. M. Minor, L. Q. Chen, J. F. Scott, L. W. Martin, and R. Ramesh, Nature **530**, 198 (2016).

[13] L. Louis, I. Kornev, G. Geneste, B. Dkhil, and L. Bellaiche, J. Phys.: Condens. Matter **24**, 402201 (2012).

[14] B.-K. Lai, I. Ponomareva, I. I. Naumov, I. A. Kornev, H. Fu, L. Bellaiche, and G. J. Salamo, Phys. Rev. Lett. **96**, 137602 (2006).

[15] Q. Zhang, L. Xie, G. Liu, S. Prokhorenko, Y. Nahas, X. Pan, L. Bellaiche, A. Gruverman, and N. Valanoor, Advanced Materials **29**, 1702375 (2017).

[16] D. Sichuga and L. Bellaiche, Phys. Rev. Lett. **106**, 196102 (2011).

[17] L. Lu, Y. Nahas, M. Liu, H. Du, Z. Jiang, S. Ren, D. Wang, L. Jin, S. Prokhorenko, C.-L. Jia, and L. Bellaiche, Phys. Rev. Lett. **120**, 177601 (2018).

[18] Y. Nahas, S. Prokhorenko, L. Louis, Z. Gui, I. Kornev, and L. Bellaiche, Nature Communications **6**, 8542 (2015).

[19] S. Das, Y. L. Tang, Z. Hong, M. A. P. Gonçalves, M. R. McCarter, C. Klewe, K. X. Nguyen, F. Gomez-Ortiz, P. Shafer, E. Arenholz, V. A. Stoica, S.-L. Hsu, B. Wang, C. Ophus, J. F. Liu, C. T. Nelson, S. Saremi, B. Prasad, A. B. Mei, D. G. Schlom, J. Íñiguez, P. Garciá-Fernandez, D. A. Muller, L. Q. Chen, J. Junquera, L. W. Martin, and R. Ramesh, Nature **568**, 368 (2019).

[20] Y. Nahas, S. Prokhorenko, I. Kornev, and L. Bellaiche, Phys. Rev. Lett. **119**, 117601 (2017).

[21] D. J. Bishop and J. D. Reppy, Phys. Rev. Lett. **40**, 1727 (1978).

[22] M. R. Beasley, J. E. Mooij, and T. P. Orlando, Phys. Rev. Lett. **42**, 1165 (1979).

[23] A. F. Hebard and A. T. Fiory, Phys. Rev. Lett. **44**, 291 (1980).

[24] S. A. Wolf, D. U. Gubser, W. W. Fuller, J. C. Garland, and R. S. Newrock, Phys. Rev. Lett. **47**, 1071 (1981).

[25] J. Frohlich and T. Spencer, Commun. Math. Phys. **81**, 527 (1981).

[26] D. J. Resnick, J. C. Garland, J. T. Boyd, S. Shoemaker, and R. S. Newrock, Phys. Rev. Lett. **47**, 1542 (1981).

[27] P. E. Lammert, D. S. Rokhsar, and J. Toner, Phys. Rev. Lett. **70**, 1650 (1993).

[28] J. Mangeri, S. P. Alpay, S. Nakhmanson, and O. G. Heinonen, Appl. Phys. Lett. **113**, 092901 (2018).

[29] S. Prosandeev, I. A. Kornev, and L. Bellaiche, Phys. Rev. Lett. **107**, 117602 (2011).

[30] P. G. de Gennes, *The physics of liquid crystals*, 2nd ed. (Clarendon, Oxford 1993).

[31] S. Chandrasekhar, *Liquid crystals* (Cambridge University Press, Cambridge 1977).

[32] L. Walizer, S. Lisenkov, and L. Bellaiche, Phys. Rev. B **73**, 144105 (2006).

[33] N. Choudhury, L. Walizer, S. Lisenkov, and L. Bellaiche, Nature **470**, 513 (2011).

[34] S. Lisenkov and L. Bellaiche, Phys. Rev. B **76**, 020102(R) (2007).

[35] S. Lisenkov, I. Ponomareva, and L. Bellaiche, Phys. Rev. B **79**, 024101 (2009).

[36] Y. Nahas, S. Prokhorenko, and L. Bellaiche, Phys. Rev. Lett. **116**, 117603 (2016)

[37] Z. Gui, L.-W. Wang, and L. Bellaiche, Nano Letters **15**, 3224 (2015).

[38] Z. Gui and L. Bellaiche, Phys. Rev. B **89**, 064303 (2014).

[39] S. Prosandeev, A. Malashevich, Z. Gui, L. Louis, R. Walter, I. Souza, and L. Bellaiche, Phys. Rev. B **87**, 195111 (2013).

[40] Q. Zhang and I. Ponomareva, Phys. Rev. Lett. **105**, 147602 (2010).

[41] D. Bimberg, M. Grundmann, and N.N. Lendentsov, *Quantum Dot Heterostructures* (Wiley , New York, 1998).

[42] D. M. Bruls, J. W. A. M. Vugs, P. M. Koenraad, H. W. M. Salemink, J. H. Wolter, M. Hopkinson, M. S. Skolnick, F. Long, and S. P. A. Gill, Appl. Phys. Lett. **81**, 1708 (2002).

[43] Yu. I. Mazur, W. Q. Ma, X. Wang, Z. M. Wang, G. J. Salamo, M. Xiao, T. D. Mishima, and M. B. Johnson, Appl. Phys. Lett., **83**, 987 (2003).

[44] Z. M. Wang, Yu. I. Mazur, G. J. Salamo, P. M. Lytvin, V. V. Strelchuk, and M. Ya. Valakh, Appl. Phys. Lett. **84**, 4681 (2004).

[45] M. Schmidbauer, Sh. Seydmohamadi, D. Grigoriev, Zh. M. Wang, Yu. I. Mazur, P. Schäfer, M. Hanke, R. Köhler, and G. J. Salamo, Phys. Rev. Lett. **96**, 066108 (2006).

[46] Z. M. Wang, K. Holmes, Yu. I. Mazur, and G. J. Salamo, Appl. Phys. Lett. **84**, 1931 (2004).

[47] Zh. M. Wang, Yu. I. Mazur, J. L. Shultz, G. J. Salamo, T. D. Mishima, and M. B. Johnson, J. Appl. Phys. **99**, 033705 (2006).

[48] S. Prosandeev and L. Bellaiche, Phys. Rev. B **77**, 060101(R) (2008).

[49] David J. Griffiths, *Introduction to Electrodynamics*, 4th Ed. (Cambridge University Press, Boston, 2017).

[50] S. Prosandeev, D. Wang, A. R. Akbarzdeh and L. Bellaiche, J. Phys.: Condens. Matter **27**, 223202 (2015).

[51] O. Tchernyshyov and G.-W. Chern, Phys. Rev. Lett. **95**, 197204 (2005).

[52] P. Shafera, P. García-Fernández, P. Aguado-Puentec, A. R. Damodarand, A. K. Yadave, C. T. Nelsond, S.-L. Hsud, J. C. Wojdeł, J. Íñiguez, L. W. Martin, E. Arenholza, J. Junquera, and R. Ramesh, PNAS **115**, 915 (2018).

[53] A. R. Damodaran, J. D. Clarkson, Z. Hong, H. Liu, A. K. Yadav, C. T. Nelson, S.-L. Hsu, M. R. McCarter, K.-D. Park, V. Kravtsov, A. Farhan, Y. Dong, Z. Cai, H. Zhou, P. Aguado-Puente, P. García-Fernández, J. Íñiguez, J. Junquera, A. Scholl, M. B. Raschke, L.-Q. Chen, D. D. Fong, R. Ramesh and L. W. Martin, Nature Materials **16**, 1003 (2017).

[54] N. Nagaosa and Y. Tokura, Nature Nanotechnology **8**, 883 (2013).

[55] A. P. Malozemoff and J. C. Slonczewski, *Magnetic Domain Walls in Bubble Materials*, First Edition, Advances in Materials and Device Research, Editor: Raymond Wolfe (Academic Press, London, 1979).

[56] A. Ruotolo, V. Cros, B. Georges, A. Dussaux, J. Grollier, C. Deranlot, R. Guillemet, K. Bouzehouane, S. Fusil and A. Fert, Nature Nanotechnology **4**, 528 (2009).

[57] T. C. Lubensky, D. Pettey, N. Currier, and H. Stark, Phys. Rev. E **57**, 610 (1998).

[58] A. Vilenkin, E. P. S. Shellard, *Cosmic strings and other topological defects* (Cambridge University Press, Cambridge, UK, 1994).

[59] S. Prokhorenko, Y. Nahas and L. Bellaiche, Phys. Rev. Lett. **118**, 147601 (2017).

[60] Y. Nahas, S. Prokhorenko, I. Kornev, and L. Bellaiche, Phys. Rev. Lett. **116**, 127601 (2016).

[61] C. Liu, J. Shen, and X. Yang, Commun. Comput. Phys. **2**, 1184 (2007).

[62] See Supplemental materials at [URL will be inserted by publisher] for the effect of the radius of the base of the $BaTiO_3$ cone on the ground state and for another interesting topological state (that is the skyrmionic tube) that can be created from the "topological eclecton".

[63] B. Xu, J. Iñiguez, and L. Bellaiche, Nat. Comm. **8**, 15682 (2017).

[64] Note that we slowly cooled down the system in order to reach the ground state, but also compared the energy of different phases and obtained by various strategies at low temperature (such as applying an electric field to get new states and then conducting further full relaxation of such new states but now under no electric field).

[65] M. G. Stachiotti and M. Sepliarsky, Phys. Rev. Lett. **106**, 137601 (2011).

[66] S. Prosandeev and L. Bellaiche, Phys. Rev. Lett. **97**, 167601 (2006).

[67] L. Lahoche, I. Luk'yanchuk, and G. Pascoli, Integrated Ferroelectrics **99**, 60 (2008).

[68] I. Ponomareva, I. I. Naumov, and L. Bellaiche, Phys. Rev. B **72**, 214118 (2005).

[69] A. P. Levanyuk and R. Blinc, Phys. Rev. Lett. **111**, 097601 (2013).

[70] M. A. P. Gonçalves, C. Escorihuela-Sayalero, P. García-Fernández, J. Junquera, J. Íñiguez, Science Advances **5**, eaau7023/1-5 (2019).

[71] I. Dzyaloshinskii, J. Phys. Chem. Sol. **4**, 241 (1958); T. Moriya Phys. Rev. **120**, 91 (1960).

FIG. 1. (color online). Macroscopic quantities obtained on cooling the investigated system as a function of temperature: (a) Supercell average of the local modes; (b) Electric toroidal moment; (c) Quadrupole moment of the density; and (d) Edwards-Anderson-like parameter. Note that error bars in our low-temperature calculations are smaller than the size of the symbols.

FIG. 2. (color online). Dipolar patterns in the (x, z)-plane defined by y=12, (y, z)-plane defined by x=12 and the (x, y)-plane defined by z=1 (and that corresponds to a basal plane of a BTO cone), as obtained at (a-c) 300K (Phase II); (d-f) 200K (Phase III); and (g-i) 10K (Phase IV), when cooling the investigated system. The center of the large magenta circles of Panels (d), (e), (g) and (h) corresponds to the core of an antivortex. The red color marks the Ti-centered dipoles at sites i for which the associated A-sites i are inside the BTO cones, while the blue color refers to Ti-centered dipoles at sites i for which the associated A-sites i are located inside the STO matrix.

FIG. 3. (color online). Dipolar structure and topology of the "topological eclecton" at 10K. Panels (a) and (b) show a schematization of the dipolar structure. Panel (a) corresponds to a general viewpoint position while Panel (b) depicts the top view from the z-axis (due to perspective, the circle corresponding to the lower cone base appears to have smaller diameter than that of the upper cone base). In both panels (a) and (b), orange arrows indicate the orientation of the dipoles on the outer surfaces of the cones. The blue triangle in panel (a) shows a (y, z) cross-section of the cones passing through the revolution axis. The in-plane projection of the dipoles located at this cross-section exhibits an antivortex at the meeting point of the cone tips schematically indicated by small black arrows in panel (a). A complete projection plot within the $(y, z)$and (x, z) planes passing through the center of the cones is shown in panel (c) where vortex and anti-vortex cores are indicated with blue and red circles, respectively. Panel (d) shows the location of hedgehog (red sphere) and anti-hedgehog (blue sphere) point defects. Panel (e1) shows the distribution of the Pontryagin charge density within the (x,y)-planes in the full supercell. Panels (e2) show the Pontraygin charge density distribution in the three (x,y) planes that host skyrmions.

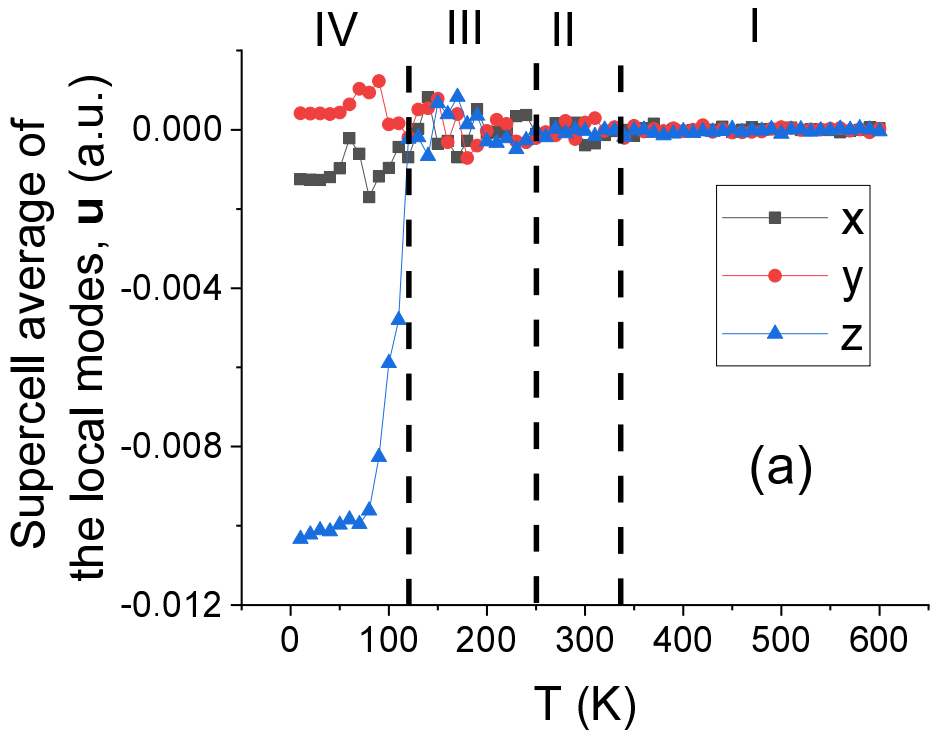
IV
III
II
I
Supercell average of the local modes, **u** (a.u.)
0.000
-0.004
-0.008
-0.012
0
100
200
300
400
500
600
T (K)
x
y
z
(a)

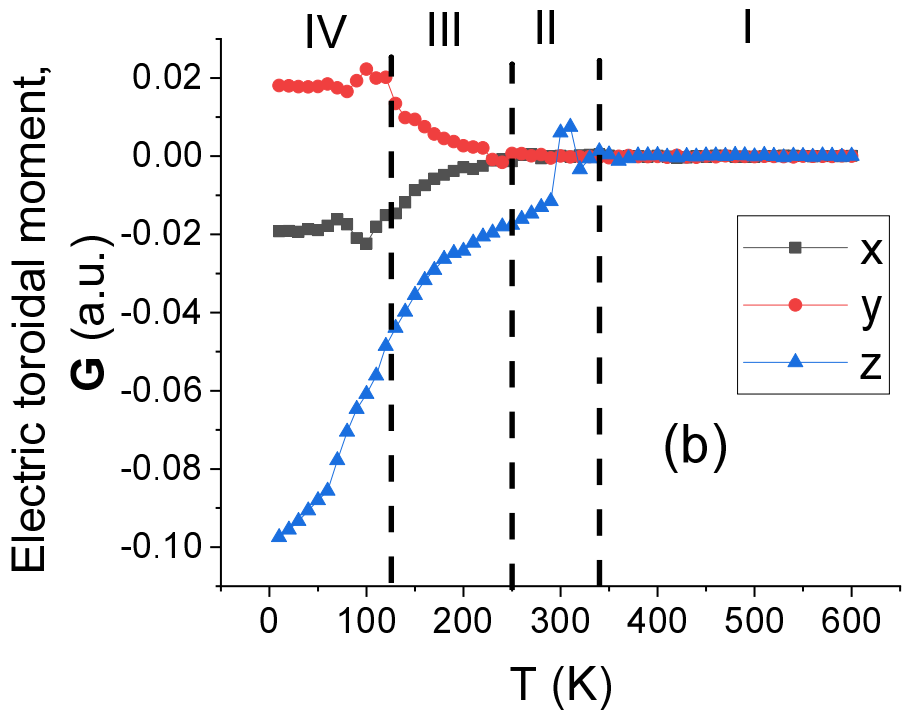
IV
III
II
I
Electric toroidal moment, **G** (a.u.)
0.02
0.00
-0.02
-0.04
-0.06
-0.08
-0.10
0
100
200
300
400
500
600
T (K)
x
y
z
(b)

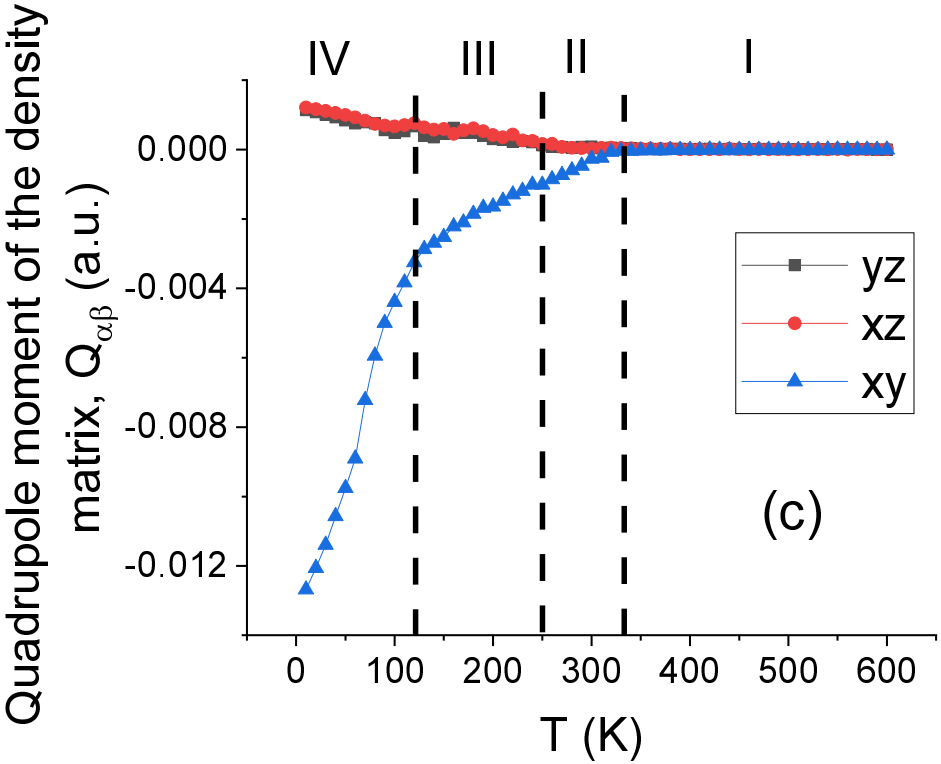
IV
III
II
I
Quadrupole moment of the density matrix, $Q_{\alpha\beta}$ (a.u.)
0.000
-0.004
-0.008
-0.012
0
100
200
300
400
500
600
T (K)
yz
xz
xy
(c)

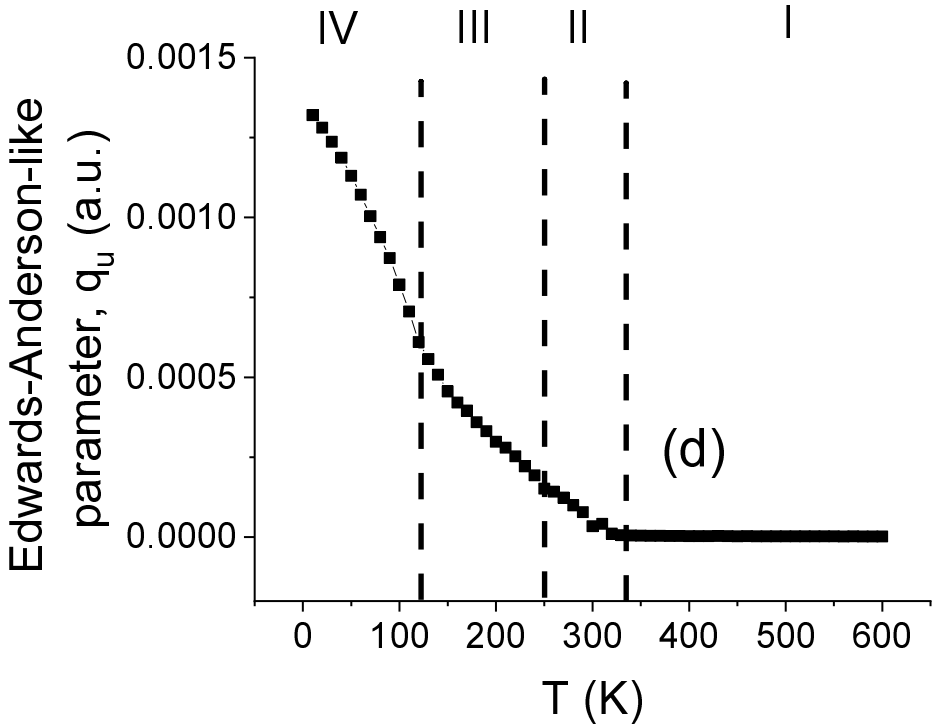
IV
III
II
I
Edwards-Anderson-like parameter, q_u (a.u.)
0.0015
0.0010
0.0005
0.0000
0
100
200
300
400
500
600
T (K)
(d)

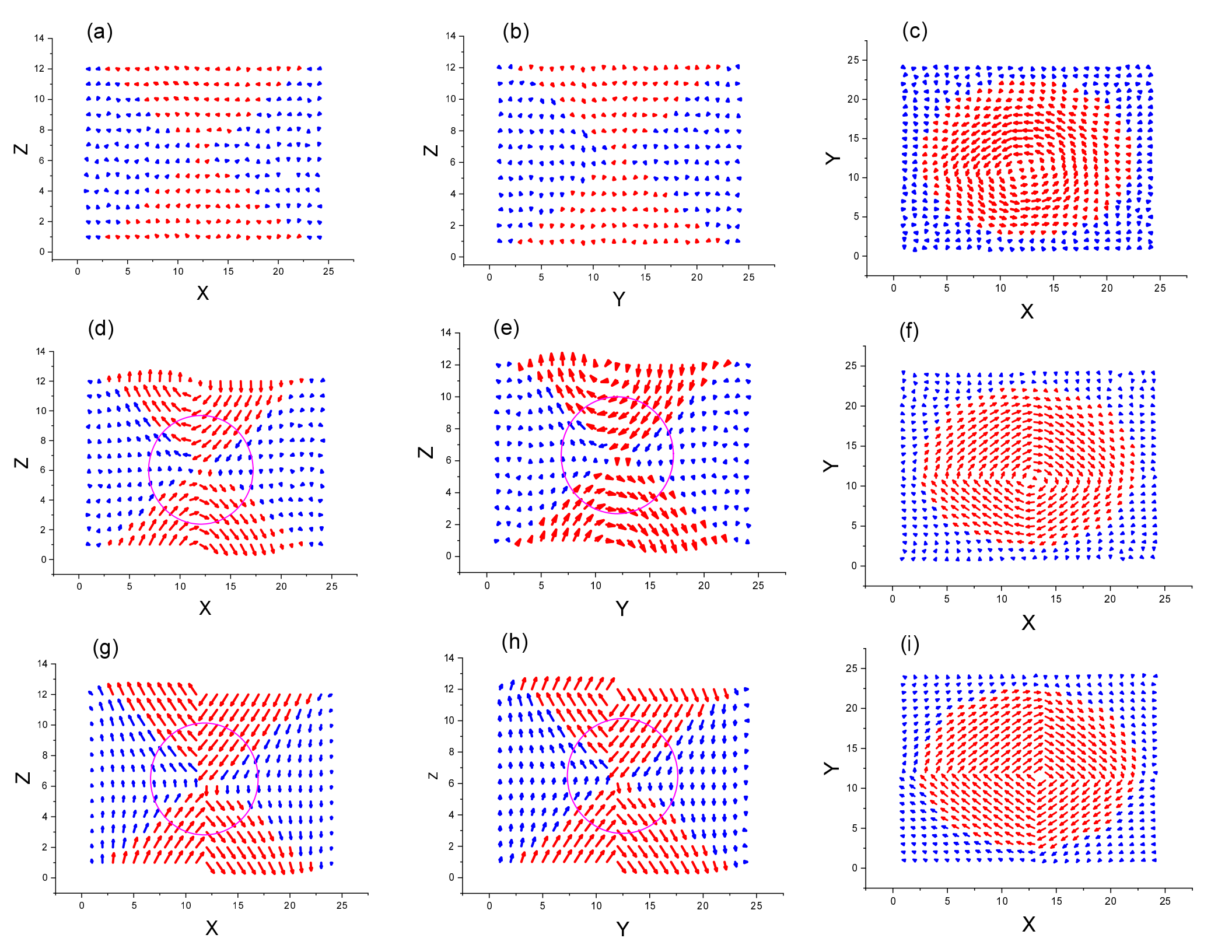
(a)
(b)
(c)
(d)
(e)
(f)
(g)
(h)
(i)
X
Y
Z

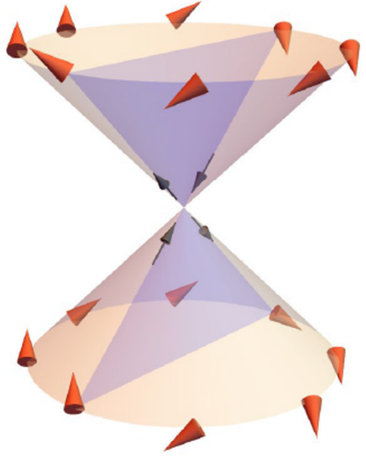

(a)

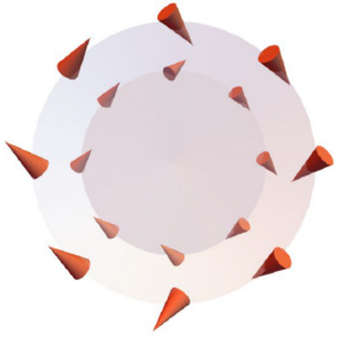

(b)

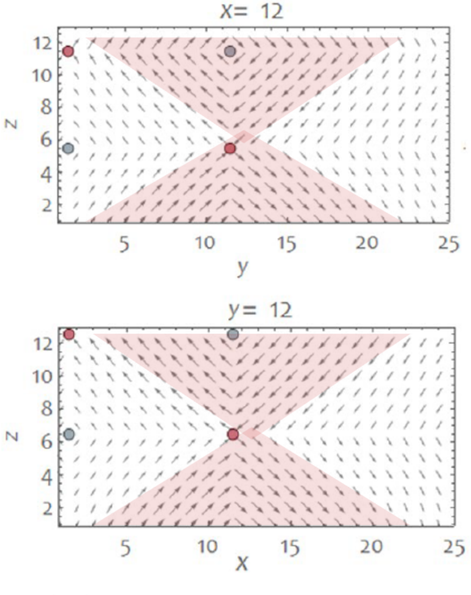

(c)

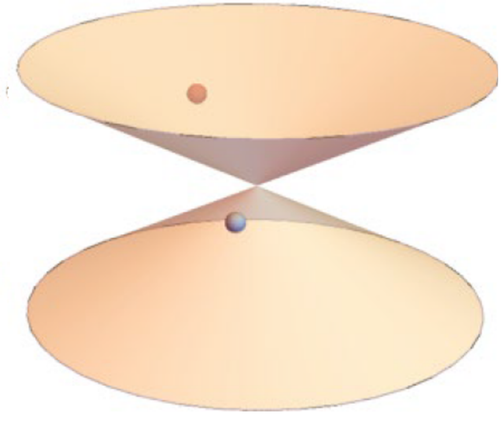

(d)

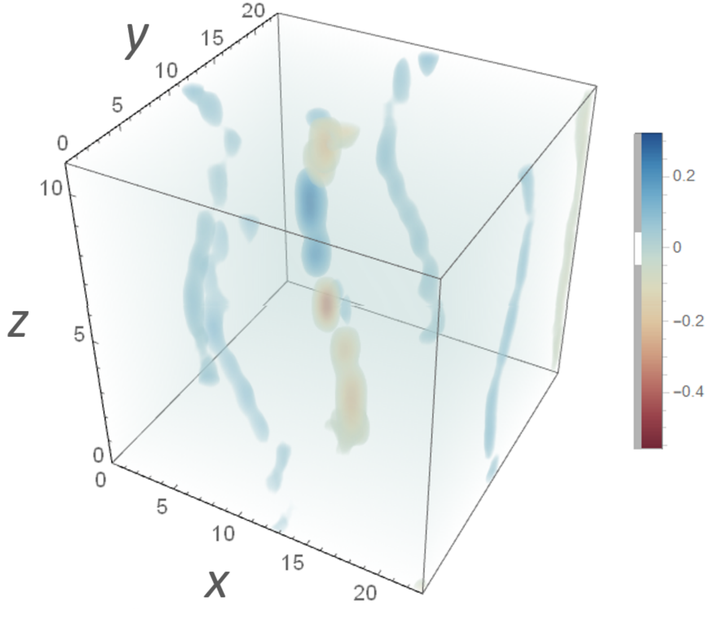

(e1)

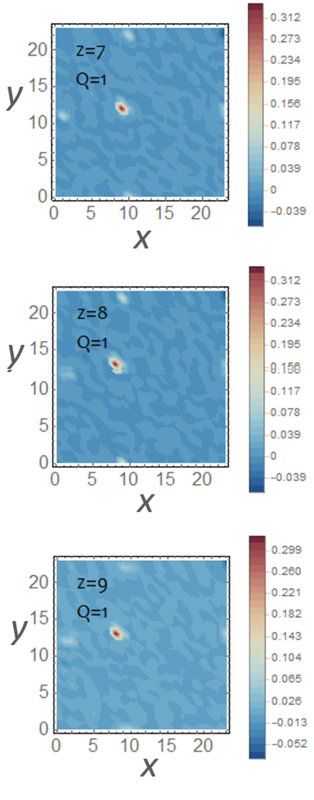

(e2)